

STELLAR POPULATIONS IN CIRCUMNUCLEAR STAR FORMING REGIONS

A. I. Díaz, M. Álvarez-Álvarez and M. Castellanos

Universidad Autónoma de Madrid, Spain

RESUMEN

Presentamos un estudio de las poblaciones estelares y las condiciones físicas del gas en Regiones Circunnucleares de Formación Estelar (CNSFR) basado en fotometría de banda ancha y estrecha y datos espectrofotométricos, que se han analizado mediante el uso de modelos evolutivos de síntesis de poblaciones y de fotoionización. Hemos encontrado que las CNSFR muestran poblaciones estelares compuestas, de edades ligeramente diferentes. Parecen tener las abundancias más altas dentro de los objetos de tipo region HII, a la vez que muestran también cocientes de N/O y S/O por encima y por debajo de los valores solares en un factor de aproximadamente 3. También, las CNSFR como clase, se segregan de la familia de regiones HII de disco, agrupándose alrededor de valores de η' menores, y por lo tanto temperaturas ionizantes más altas.

ABSTRACT

We present a study of the stellar populations and gas physical conditions in Circumnuclear Star Forming Regions (CNSFR) based on broad and narrow band photometry and spectrophotometric data, which have been analyzed with the use of evolutionary population synthesis and photoionization models. It is found that most CNSFR show composite stellar populations of slightly different ages. They seem to have the highest abundances in HII region-like objects, showing also N/O overabundances and S/O underabundances by a factor of about three. Also, CNSFR as a class, segregate from the disk HII region family, clustering around smaller η' values, and therefore higher ionizing temperatures.

Key Words: **ISM: H II REGIONS — STARS: IONIZING POPULATIONS**

1. INTRODUCTION

The inner parts of some spiral galaxies show higher star formation rates than usual and this star formation is frequently arranged in a ring or pseudoring pattern around their nuclei. This fact seems to correlate with the presence of bars and, in fact, computer models which simulate the behavior of gas in galactic potentials have shown that nuclear rings may appear as a consequence of matter infall owing to resonances present at the bar edges (Combes & Gerin 1985; Athanassoula 1992).

In general, Circumnuclear Star Forming Regions (CNSFR), also referred to as “hotspots”, are alike luminous and large disk HII regions, but look more compact and show higher peak surface brightness (Kennicutt et al. 1989). In many cases they contribute substantially to the emission of the entire nuclear region.

Their large H α luminosities, typically higher than 10^{39} erg s $^{-1}$ points to relatively massive star clusters as their ionization source, which minimizes the uncertainties due to small number statistics when applying population synthesis techniques (see e.g.

Cerviño et al. 2002). These regions then constitute excellent places to study how star formation proceeds in circumnuclear environments.

To this aim, we have combined broad-band photometry, narrow-band Balmer emission imaging and spectrophotometric data for a sample of CNSFR whose analysis can provide detailed information about both ionizing and non-ionizing stellar populations.

2. OBSERVATIONS AND DATA SAMPLE

2.1. Photometric Data

Two data sets of broad and narrow band photometry were obtained. The first one with the JKT telescope in the Observatory of the Roque de los Muchachos (ORM, La Palma, Spain), in the V,R,I and H α filters included four galaxies. The details concerning this first set of data can be found in Díaz et al. (2000). In the second one, with the 1.52 m Spanish Telescope in Calar Alto Observatory (Almería, Spain), the sample was enlarged to 20 galaxies and the filters used were U,B,R,I, H α and H β . Spatial resolution is about 0.33 arcsec/pix.

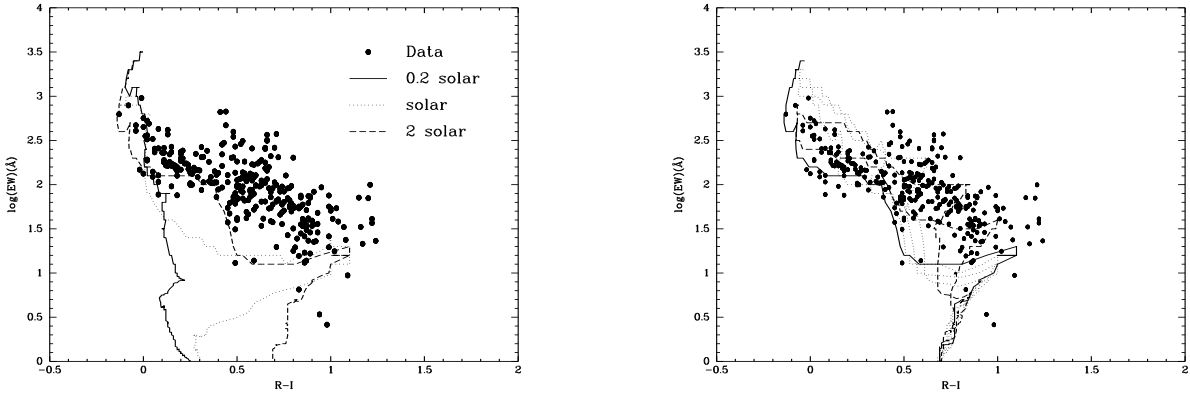


Fig. 1. Relative intensity (left) and equivalent width (right) of the WR blue ‘bump’ *versus* $H\beta$ equivalent width for SV98 models of three different metallicities as labelled. The data are shown as solid and open symbols as explained in the text.

The observed galaxies are bright ($14.1 > B > 9.6$) and nearby ($8.4 < D \text{ (Mpc)} < 37.2$) yielding linear scales between 41 and 181 pc/arcsec. They are spirals of different morphological type. 70% of them are barred (20% strongly and 50% weakly) and 25% are unbarred. No information is available for the remaining 5%. Regarding interaction, 60% of them have a neighboring galaxy closer than 4 arcmin and 40% do not. Finally, 65% of the sample harbour an active nucleus: 10% Sey1, 40% Sey2, 15% LINER, 30% shows HII region nuclei and 5% do not show any signs of nuclear activity.

A total of 332 CNSFR in the sample galaxies have been measured and analyzed.

2.2. Spectroscopic Data

Regarding spectrophotometry, we have analyzed data of moderate resolution ($1.4 - 2.5 \text{ \AA/pix}$) and wide coverage (3500 to 9700 \AA) obtained with the INT and WHT telescopes (ORM). More details on these observations can be found in Pérez-Olea (1996) and Álvarez-Álvarez et al. (2001). These configurations allow the observation of both the bright oxygen ([OII] and [OIII]) and sulphur ([SII] and [SIII]) emission lines necessary for the diagnostics of the emitting gas.

3. ANALYSIS OF BROAD-BAND COLORS: STELLAR POPULATION SYNTHESIS MODELS

The broad band colors have been analyzed in combination with the $H\alpha$ equivalent widths obtained through narrow filters, with the use of the stellar population synthesis models by Leitherer et al (1999; STB99). These models give predictions for stellar

populations of different metallicities (between 0.05 and 2 times solar) and initial mass functions (power laws with exponent $\alpha = 2.35, 3.00$, upper mass limit $m_{up} = 100, 30 M_{\odot}$ and lower mass limit $m_{low} = 1 M_{\odot}$). The observed colors have been corrected for reddening using the observed $H\alpha/H\beta$ ratio. Both single burst and continuous star formation are considered.

In our analysis we have assumed that the $H\alpha$ emission comes from the ionizing stars while the contribution of any underlying stellar population should be detectable as emission in continuum light, mostly at the longer wavelengths (redder colors). Figure 1 (left panel) shows the equivalent width of $H\alpha$, $EW(H\alpha)$, *versus* the (R-I) colour for the observed regions. Single burst stellar populations for a Salpeter initial mass function and different metallicities: 0.2 solar, solar and twice solar are overimposed. It can be seen that only a small fraction of the observed objects (the very blue ones with high values of $EW(H\alpha)$ and the very red ones with low values of $EW(H\alpha)$) can be reproduced by the models. Continuous star formation provides even worse results. The great majority of the regions can be explained only by the combination of at least two populations of different ages. In order to explore this possibility, we have constructed models of two populations of the same metallicity and slightly different ages, combined according to two parameters: t , which represents the difference in age of the two assumed populations, and f , which represents the ratio between the mass of the youngest population and the total mass of the region. Models of this kind are shown in Figure 1 (right panel) to be able to reproduce the observations in the $EW(H\alpha)$ - (R-I) plot. This situation

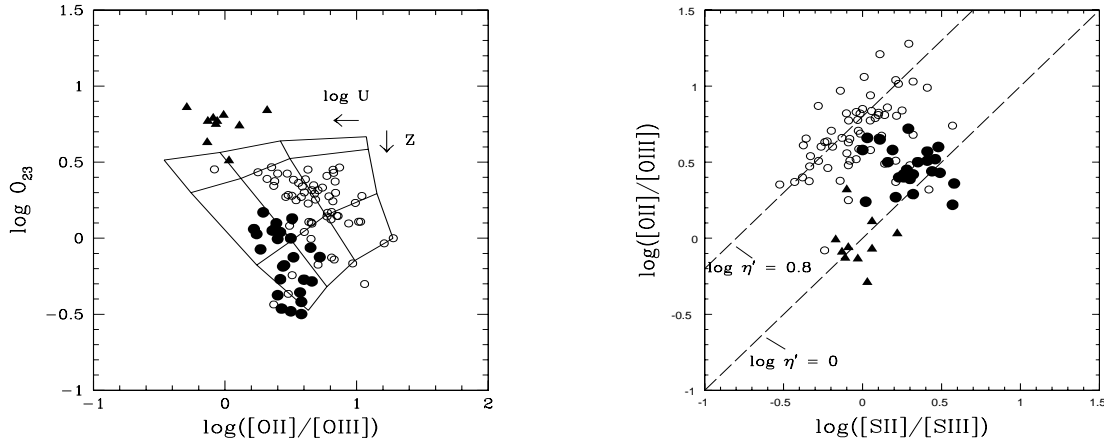


Fig. 2. The $\log O_{23}$ vs $\log([OII]/[OIII])$ (left panel) and $\log([OII]/[OIII])$ vs $\log([SII]/[SIII])$ (right panel) diagnostic diagrams. Solid symbols correspond to CNSFR of low (triangles) and high (circles) metallicity. Open symbols are high metallicity disk HII regions from the samples of Bresolin et al. (1999) and Díaz & Pérez-Montero 2000. Continuous lines show the predictions of photo-ionization models as explained in the text.

looks however more complicated when the (U-B) colors are considered in the analysis. Not even the composite population models are able to reproduce the location of the HII regions in the (U-B)-(R-I) diagram, with about half of the regions showing (U-B) colors much redder than any model prediction. This fact needs to be studied further both from the observational and theoretical sides in order to understand how star formation takes place in these HII regions.

4. ANALYSIS OF EMISSION LINE SPECTRA: PHOTO-IONIZATION MODELS

The emission line data have been analyzed with the use of photo-ionization models (CLOUDY; Ferland 1999). We have modelled the HII regions using the simplest hypotheses: a single ionizing star, spherical symmetry, uniform chemical composition and constant particle density. Any effects due to the presence of dust have not been considered, except for the depletion of refractory elements by a factor of ten. We have assumed the emission line spectrum of the HII region to be controlled by the spectral energy distribution of the ionizing star, which has been represented by Mihalas' atmosphere models of different effective temperatures, the geometrical factors, represented by the ionization parameter, U , and the chemical composition of the gas, represented by its oxygen abundance relative to hydrogen, O/H . The comparison of model predictions and data has been made with the use of diagnostic diagrams.

Figure 2 (left panel) shows the abundance parameter $\log O_{23} = ([OII] + [OIII])/H\beta$ versus the ionization parameter indicator $\log([OII]/[OIII])$. Observed

CNSFR are represented as solid symbols, triangles for regions in NGC 3310 and NGC 7714 known to have a subsolar oxygen abundance (Pastoriza et al. 1993, González Delgado et al. 1995), and circles for the rest of the analyzed galaxies: NGC 1068, NGC 2903, NGC 3351, NGC 3504 and NGC 5953. These latter regions have solar or oversolar metallicity according to the empirical criterion of Díaz & Pérez-Montero (2000), *i.e.* $O_{23} \leq 0.47$ and $-0.5 \leq S_{23} \leq 0.28$ ¹. As a comparison sample, open circles represent disk HII regions from the samples of Díaz & Pérez-Montero (2000) and Bresolin et al. (1999) which meet the same criterion. The lines in the diagram correspond to photoionization models of the same effective temperature (37000 K) and different ionization parameter (from -2.0 to -3.5) and O/H abundance (from 0.7 to 3 times solar). It can be seen that most high metallicity CNSFR have O/H abundances higher in average than their disk counterparts although they show comparable $[OII]/[OIII]$ ratios. CNSFR also segregate from the disk HII regions in the $([OII]/[OIII])$ versus $([SII]/[SIII])$ diagram (Figure 2, right panel). The former cluster around the value of $\log \eta' = 0.0$ while the latter do around $\log \eta' = 0.8$. This parameter, η' is a measure of the hardness of the ionizing radiation (see Vílchez & Pagel 1988) and seems to imply higher ionizing temperatures for the CNSFR.

Regarding relative abundances, some peculiarities are observed concerning both nitrogen and sulphur. These can be visualized in Figure 3. In the

¹The sulphur abundance parameter S_{23} is defined as $\log S_{23} = ([SII] + [SIII])/H\beta$

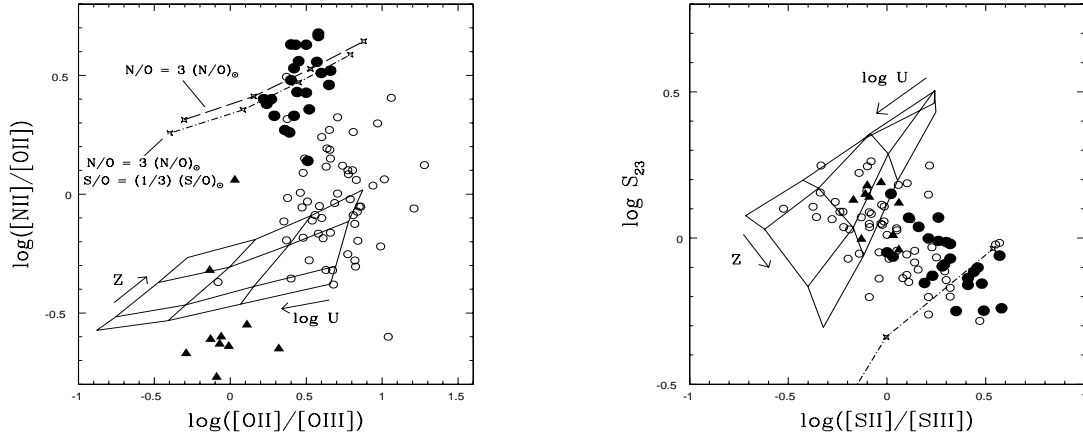


Fig. 3. The $\log([NII]/[OII])$ vs $\log([OII]/[OIII])$ (left panel) and $\log S_{23}$ vs $\log([SII]/[SIII])$ (right panel) diagnostic diagrams. Symbols are as in the previous figure.

left panel we can see the location of the CNSFR in the $\log([NII]/[OII])$ versus $\log([OII]/[OIII])$ diagram. The high metallicity CNSFR look clearly overabundant in nitrogen in comparison to disk HII region, which is compatible with their apparent higher metallicity. The continuous lines in the diagram show the same photoionization models as in Figure 2. For these models the N/O ratio has been kept to its solar value. The dashed line, however, shows models with O/H and N/O 3 times their solar values. The right panel shows the position of the CNSFR in the $\log S_{23}$ versus $\log([SII]/[SIII])$ diagram. A trend of decreasing S_{23} and increasing $[SII]/[SIII]$ seems to be defined by the data points, which could be interpreted, in principle, as an increase in metallicity and a corresponding decrease in ionization parameter. This trend however cannot be reproduced by the models with solar relative abundances which are shown, again, as continuous lines. The only way to reproduce the location of the CNSFR implies a reduction of the S/O abundance by a factor of about 3, as shown by the dashed-dotted line. This reduction does not affect the $[NII]/[OII]$ and $[OII]/[OIII]$ ratios as can be seen in the left panel.

This work has been partially supported by DGI-CYT project AYA-2000-0973.

REFERENCES

- Álvarez-Álvarez, M., Díaz, A. I., Terlevich, E., Terlevich, R., Pastoriza, M. G., & Dottori, H. A. 2001, *Highlights of Spanish Astrophysics II*, 363.
- Athanassoula, E., 1992, *MNRAS*, 259, 345.
- Bresolin, F., Kennicutt, R. C., & Garnett, D. R. 1999, *ApJ*, 510, 104.
- Cerviño, M., Valls-Gabaud, D., Luridiana, V., & Mas-Hesse, J. M. 2002, *A&A*, 381, 51.
- Combes, F. & Gerin, M. 1985, *A&A*, 150, 327.
- Díaz, A. I. & Pérez-Montero, E. 2000, *MNRAS*, 312, 130.
- Díaz, A. I., Álvarez, M., Álvarez, Terlevich, E., Terlevich, R., Portal, M. S. ;., & Aretxaga, I. 2000, *MNRAS*, 311, 120.
- Ferland, G. 1999, *HAZY: A Brief Introduction to CLOUDY* (Lexington: Univ. Kentucky Press)
- Gonzalez-Delgado, R. M., Perez, E., Diaz, A. I., Garcia-Vargas, M. L., Terlevich, E., & Vilchez, J. M. 1995, *ApJ*, 439, 604.
- Kennicutt, R. C., Keel, W. C., & Blaha, C. A. 1989, *AJ*, 97, 1022.
- Leitherer, C. et al. 1999, *ApJS*, 123, 3.
- Pastoriza, M. G., Dottori, H. A., Terlevich, E., Terlevich, R., & Díaz, A. I. 1993, *MNRAS*, 260, 177.
- Pérez-Olea, D. 1996, Ph.D. Thesis, Universidad Autónoma de Madrid.
- Vilchez, J. M. & Pagel, B. E. J. 1988, *MNRAS*, 231, 257.

A. I. Díaz, M. Álvarez-Álvarez and M. Castellanos: Depto. Física Teórica, C-XI, Universidad Autónoma de Madrid, 28049 Madrid, España (angeles.diaz@uam.es, malvar4@roble.pntic.mec.es, marcelo.castellanos@uam.es).